



Mobility of point defects in CoCrFeNi-base high entropy alloys

Naoyuki Hashimoto^{a,*}, Yuta Ono^b

^a Faculty of Engineering, Hokkaido University, Sapporo, 060-8628, Japan

^b Graduate School of Engineering, Hokkaido University, Sapporo, 060-8628, Japan



ARTICLE INFO

Keywords:

High entropy alloy
In-situ irradiation
Precipitation
Positron annihilation
Point defect mobility
Transmission electron microscope

ABSTRACT

The in-situ observation of microstructural evolution under electron irradiation was performed in order to experimentally estimate the mobility of vacancy and interstitial in 316 stainless steel and CoCrFeNi-base high entropy alloys. The vacancy migration energy in CoCrFeNiMn and CoCrFeNiAl_{0.3} was estimated to be lower and higher compared with that in 316 stainless steel, respectively. While, the interstitial migration energy in those alloys seems to be almost the same. The increase in vacancy migration energy in CoCrFeNiAl_{0.3} is probably due to a strong interaction between vacancy and Al. The positron annihilation analysis revealed that vacancies might exist close to Co and Ni atoms in CoCrFeNi-base high entropy alloys. In addition, vacancies could also be captured by Mn and Al atoms in CoCrFeNiMn and CoCrFeNiAl_{0.3}, respectively. The electron- and ion-irradiation at 400 and 300 °C up to 1.5 dpa resulted in the precipitation of the intermetallic compounds, such as CoFe, NiFe in CoCrFeNiMn, and Ni₃Al in CoCrFeNiAl_{0.3}. From these results, it is suggested that Co, Ni, Mn, and Al atoms could affect the vacancy mobility in HEAs, leading to the delay of microstructural evolution and the enhancement of precipitation under irradiation.

1. Introduction

High Entropy Alloy (HEA) is an alloy in which multi-component elements are configured in almost equal ratios, unlike alloys in which a small amount of one or two elements is added to the main elements like conventional alloys. HEA is characterized by the random arrangement of atoms. Several HEAs form ductile solid solution structures involving face centered cubic (FCC) or body centered cubic (BCC) phases or mixtures of the two, instead of brittle intermetallic compounds [1–4]. It has been reported that some HEAs have unique properties such as a high strength and high radiation resistance at elevated temperatures compared with conventional alloys [5–7]. Those attractive physical and mechanical properties make HEAs potential candidates for high temperature fission or fusion structural applications. However, the studies on their radiation resistance at elevated temperatures relevant for potential nuclear energy applications is limited. It is hypothesized that the high mixing entropy of HEAs might influence point defect recombination in irradiated materials by modifying the distance of vacancy-interstitial recombination interaction, solute diffusivity, and other mechanisms, thereby producing different radiation stability compared to conventional single-phase alloys. Currently available austenitic stainless steels for light water reactors (LWRs) do not appear to exhibit sufficient radiation damage

resistance for extended operation at elevated temperatures in next generation nuclear energy systems [8,9]. Therefore, in this study, we focused on the mobility of the point defects and microstructural changes in FCC-type high entropy alloys irradiated at elevated temperatures.

2. Experimental procedure

The materials used in this study are three of FCC-type single phase materials; CoCrFeNiMn-HEA, CoCrFeNiAl_{0.3}-HEA [10,11], and 316 austenitic stainless steel (316SS). Two HEAs were prepared by induction furnace in high-purity argon atmosphere. The compositions of three alloys are listed in Table 1. The HEAs were solution annealed at 800 °C for 24 h, and then 3 mmφ TEM disks were punched out for the irradiation experiments. The disk specimens were electro-polished for electron irradiation experiment or etched for the ion irradiation experiment. In addition, the plate samples (7 mm × 7 mm × 1 mm) were provided for the positron annihilation measurement. Electron irradiation and in-situ observation were performed using a high voltage electron microscope (HVEM), JEM-ARM-1300 (JEOL) operated at 1250 kV at Hokkaido University. The dose rates were from 2.0×10^{-4} to 3.0×10^{-3} dpa/s. The dose rates were selected to minimize the sink effect from the specimen surface and other dislocation loops. The migration energies of

* Corresponding author.

E-mail address: hasimoto@eng.hokudai.ac.jp (N. Hashimoto).

Table 1

The nominal chemical composition of the prepared High Entropy Alloys.

Alloys	Fe	Cr	Ni	Mn	Co	Al	Mo	V	C	N
316 SS (wt%)	Bal.	17.22	13.24	2.03	–	–	2.40	0.04	0.066	–
CoCrFeNiMn (at%)	19.99	19.99	19.99	19.99	19.99	–	–	–	0.007	<0.0009
CoCrFeNiAl _{0.3} (at%)	23.29	23.29	23.29	–	23.29	6.79	–	–	0.005	<0.0009

Table 2

Condition of the electron- and Fe³⁺ ion-irradiation experiments.

	Electron irradiation	Fe ³⁺ ion irradiation
Accel. Voltage	1250 kV	6.4 MeV
Temperature	460–600 °C	300 °C
Dose	1.5 dpa	1.0 dpa

vacancies (E_v) and interstitials (E_i) can be expressed by the rate theory [12,13]. The motion of point defects when vacancies and interstitials are balanced at vacancy mobile temperatures is governed by the vacancy mobility. Therefore, the irradiation temperature was set to be high enough for vacancy motion (from 450 °C to 600 °C); thus the vacancy–interstitial mutual annihilation occurred due to the effective mobility of vacancies. Fe³⁺ ion-irradiation experiments were performed using Dual-Beal Facility at Energy Science and Technology in Kyoto University. Table 2 summarizes the irradiation conditions. Furthermore, the positron annihilation measurements were performed in order to investigate the vicinity of lattice defects in the HEAs. TEM observation and the elemental mapping were performed for the irradiated samples using a Cs-corrected scanning transmission electron microscope (Titan3 G2 60–300) at Hokkaido University. Cross-section transmission electron microscopy (TEM) specimens from the ion-irradiated samples were prepared using a focus ion beam (FIB) (JEOL JIB 4600F) system with Ga⁺ ions. The ion energy at the main thinning step was 30 keV, and during

the later stages of thinning, the energy was reduced to 10 keV with the final thinning at a foil thickness of ~100 nm performed with a current of 30 pA.

3. Results and discussion

3.1. Estimation of vacancy migration energy

All the prepared samples remained fully crystalline and retained their original FCC phase with no detectable second phase observed as a function of irradiation temperature and dose up to 1.5 dpa. The 316SS, CoCrFeNiMn, and CoCrFeNiAl_{0.3} were electron-irradiated at 1×10^{-4} dpa/s with temperature stepwisely from 500 to 460 °C, 600 to 560 °C, and 460 to 500 °C, respectively. In this irradiation condition, both interstitials and vacancies can move appreciably. Microstructural evolution in each alloy under electron irradiation was shown in Fig. 1. Electron irradiation introduced point defects in the alloys, and then, microstructural evolution such as the formation and the growth of self-interstitial atom (SIA) cluster (black dots), SIA faulted loops (Frank loops), and SIA perfect loops were observed with increasing irradiation time. Irradiation-induced microstructure of the alloys seemed similar, however, the growth rate of those loops in each alloy was very different. As seen in Fig. 1, the growth rate of SIA perfect loops in CoCrFeNiMn and CoCrFeNiAl_{0.3} was the highest and the lowest, respectively. It is also noted that the number density of SIA perfect loops in 316SS was one

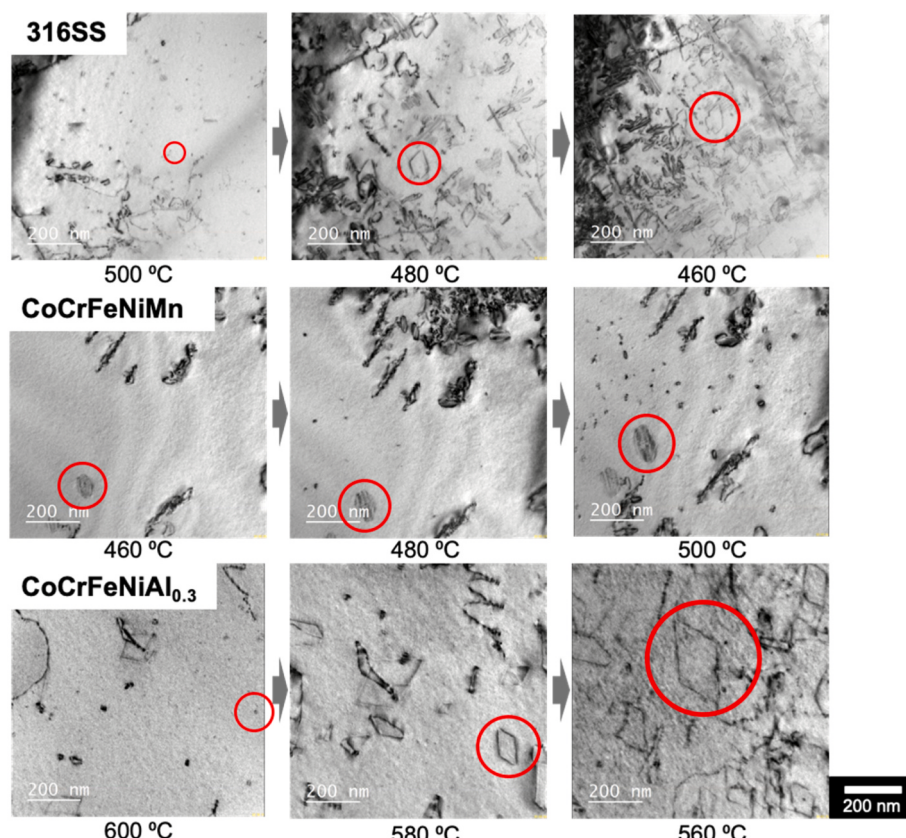


Fig. 1. Typical sequences of dislocation loop growth in 316SS, CoCrFeNiMn, and CoCrFeNiAl_{0.3} during electron irradiation for 5 min at each temperature.

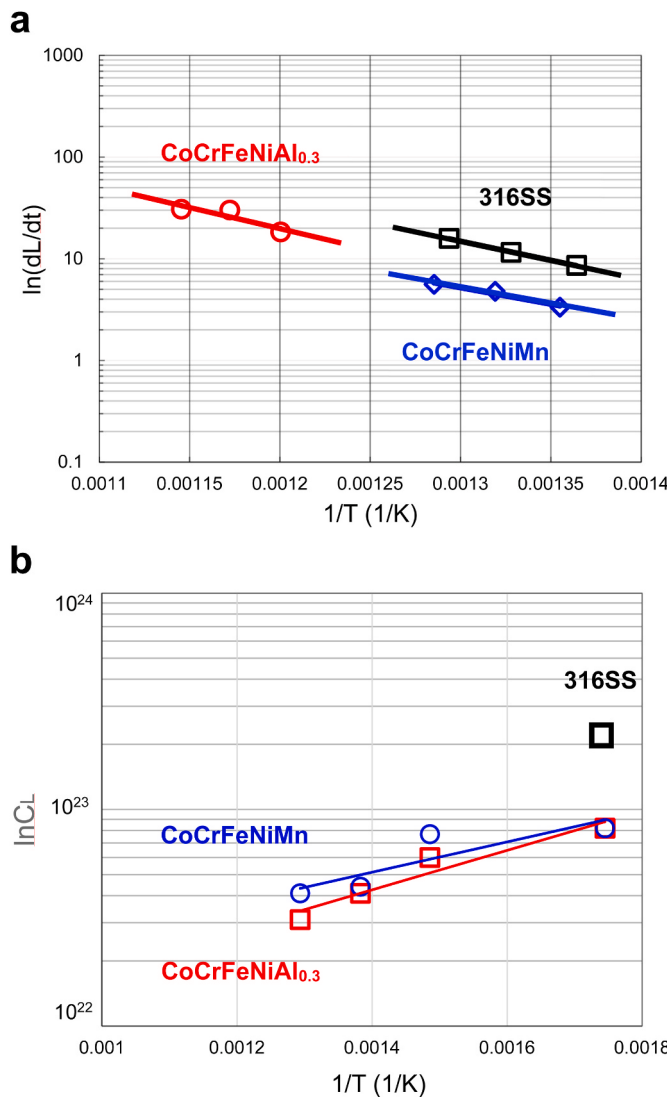


Fig. 2. Arrhenius plots of (a) loop growth rate and (b) loop number density in electron-irradiated 316SS, CoCrFeNiMn, and CoCrFeNiAl_{0.3}. The loop number density in 316SS at 300 °C was also added in (b).

order higher than that in HEAs. This different might be explained by the different of stacking fault energy (SFE) between 316SS and the HEAs. According to a previous study on the relationship between SIA loop formation and SFE based on the density functional theory (DFT) calculation [14], the number of SIA perfect loops would be higher at lower SFE, leading to an increase in the ratio of glissile SIA clusters with a decrease in SFE. Therefore, the highest loop number density in 316SS would be probably due to the lower SFE compared to the HEAs.

At temperatures at which vacancies are mobile, interstitial clusters grow into well-defined dislocation loops as shown in Fig. 1. In the case of high vacancy mobility, the vacancy-interstitial mutual annihilation reaction due to the motion of vacancies becomes effective when the vacancies accumulate in the matrix [12]. Saturation of both vacancies and interstitials will be established, and then, the motion efficiency: the product of the concentration and mobility, for interstitials and vacancies are equal. This motion efficiency is determined solely by the mobility of vacancies and is independent of that of interstitials, as long as the motion of interstitials is much faster than that of vacancies. The migration energies of vacancies (E_v) and interstitials (E_i) can be estimated by the equations proposed by Refs. [12,13]. At steady state, migration energies of both types of point defects are given as follows:

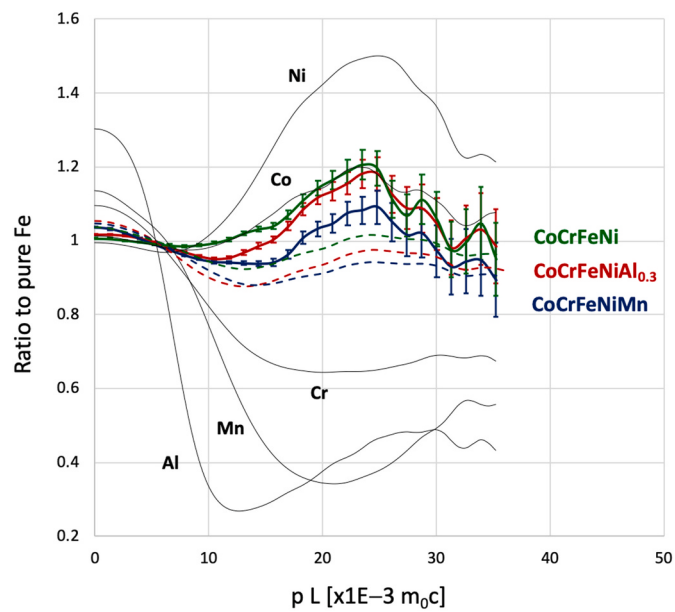


Fig. 3. Ratio curve of each alloy to pure iron by positron annihilation measurements. (The dotted line is the calculation result obtained from the ratio curve of each single element to pure iron, and the solid line is the experimental result obtained from the prepared alloy.)

$$\ln\left(\frac{dL}{dt}\right) = C_2 - \frac{E_v^M}{2kT}$$

$$C_{LS} = C_3 \exp\left(-\frac{E_i^M}{2kT}\right)$$

where C_2 and C_3 are constants, and L , k , T , and C_{LS} denote the length of dislocation loops, Boltzmann constant, absolute temperature, and the saturated number density of dislocation loops, respectively. Using these equations, migration energy of vacancy and interstitial can be estimated by measuring loop growth rate at an appropriate temperature range. Fig. 2 shows Arrhenius plots of (a) loop growth rate and (b) loop number density in all the alloys at each irradiation temperature. The loop number density in 316SS at 300 °C was also added in Fig. 2(b). Electron irradiation experiments in 316SS, CoCrFeNiMn, and CoCrFeNiAl_{0.3} indicated the apparent vacancy migration energy to be 1.5, 0.8, and 1.6 eV, respectively. On the other hand, the interstitial migration energies in CoCrFeNiMn and CoCrFeNiAl_{0.3} were estimated to be 0.28 and 0.36 eV, respectively. In general, the loop formation energy is independent on the migration energy of point defects, therefore, the change in interstitial migration energy does not affect the loop formation behavior. The different of migration energy between interstitial and vacancy would affect the loop growth behavior. The loop growth rate is proportional to the difference of flux between interstitials and vacancies. In this study, therefore, the growth of Frank loop in CoCrFeNiAl_{0.3} was faster than that in CoCrFeNiMn. The difference of E_v between CoCrFeNiMn, and CoCrFeNiAl_{0.3} would be due to the difference of interaction between Mn or Al and vacancy. A previous study [15] reported that the vacancy migration energy of Fe–8Cr–5Al was experimentally estimated to be higher than that in Fe–8Cr. Furthermore, a theoretical approach by DFT also indicated a higher vacancy migration energy in the Al-contained ferritic steels [15]. It was suggested that a strong interaction between Al and vacancy would lead to the suppression of vacancy motion. This would be a possible reason of the increase in vacancy migration energy in CoCrFeNiAl_{0.3} compared with that in CoCrFeNiMn. However, the Al effect on the vacancy migration energy in the ferritic steel could not explain the behavior in HEAs. The other experimental approach such as the positron annihilation measurement would be needed on this issue.

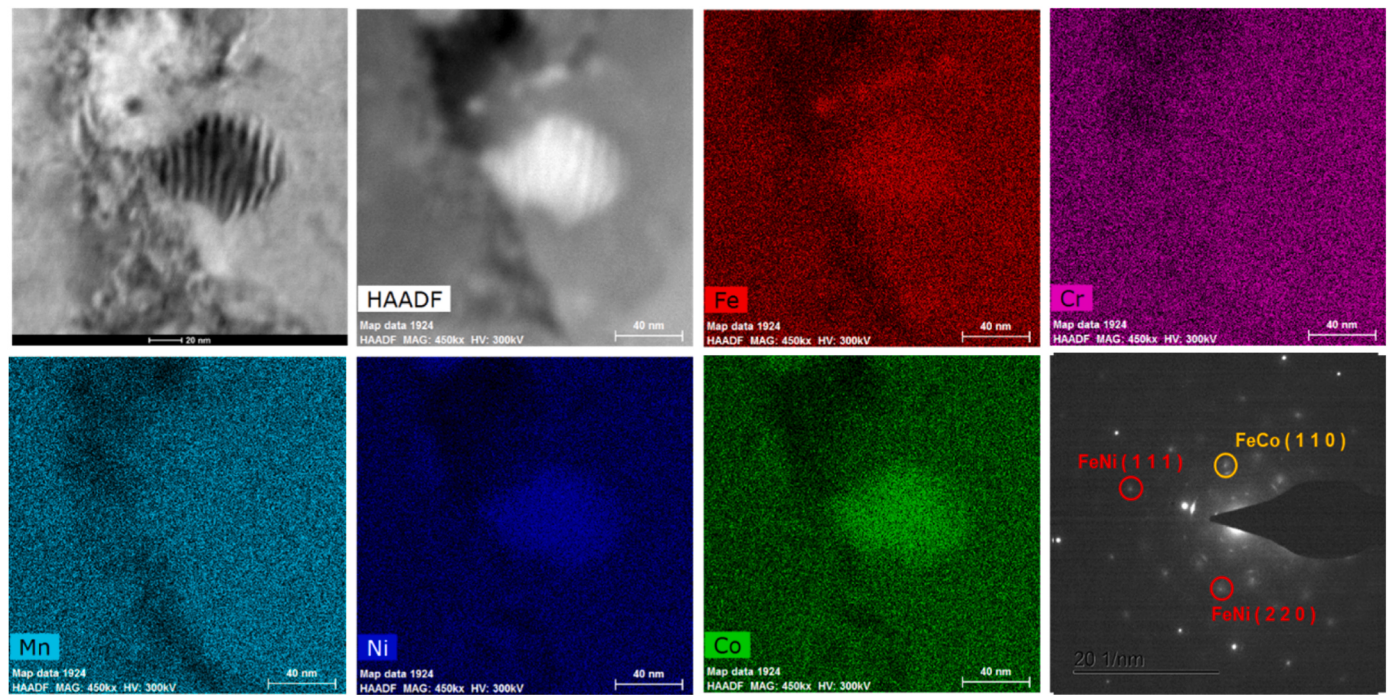


Fig. 4. Element mapping and diffraction pattern of CoCrFeNiMn HEA after electron irradiation at 400 °C and 1.5 dpa.

3.2. Positron annihilation measurement for HEAs

The positron annihilation measurement method is a technique for measuring the momentum distribution of inner-shell electrons by precisely and simultaneously measuring the energy of annihilation γ rays emitted by annihilation between an electron and a positron. Since the momentum distribution of the core electrons is unique to the element, the element to which the positron annihilation partner belongs can be identified. Positrons heat and diffuse before pair annihilation and are trapped at specific sites. Therefore, elemental analysis of positron

capture sites such as composite materials in which vacancies are combined with impurities and solutes, and nanoprecipitates embedded in crystals is possible [16]. Fig. 3 shows the results of positron annihilation measurements with the momentum on the horizontal axis and the ratio to pure iron on the vertical axis. The dotted lines exhibit the ratios of each element to iron, and the solid lines are the actual measurement for each element. For example, looking at the red lines indicating the non-irradiated CoCrFeNiMn, the solid line shows higher intensity than the dotted line in the 10–30 momentum region. It is noted that the lines of Co and Ni show higher intensity in the 10–30 momentum region.

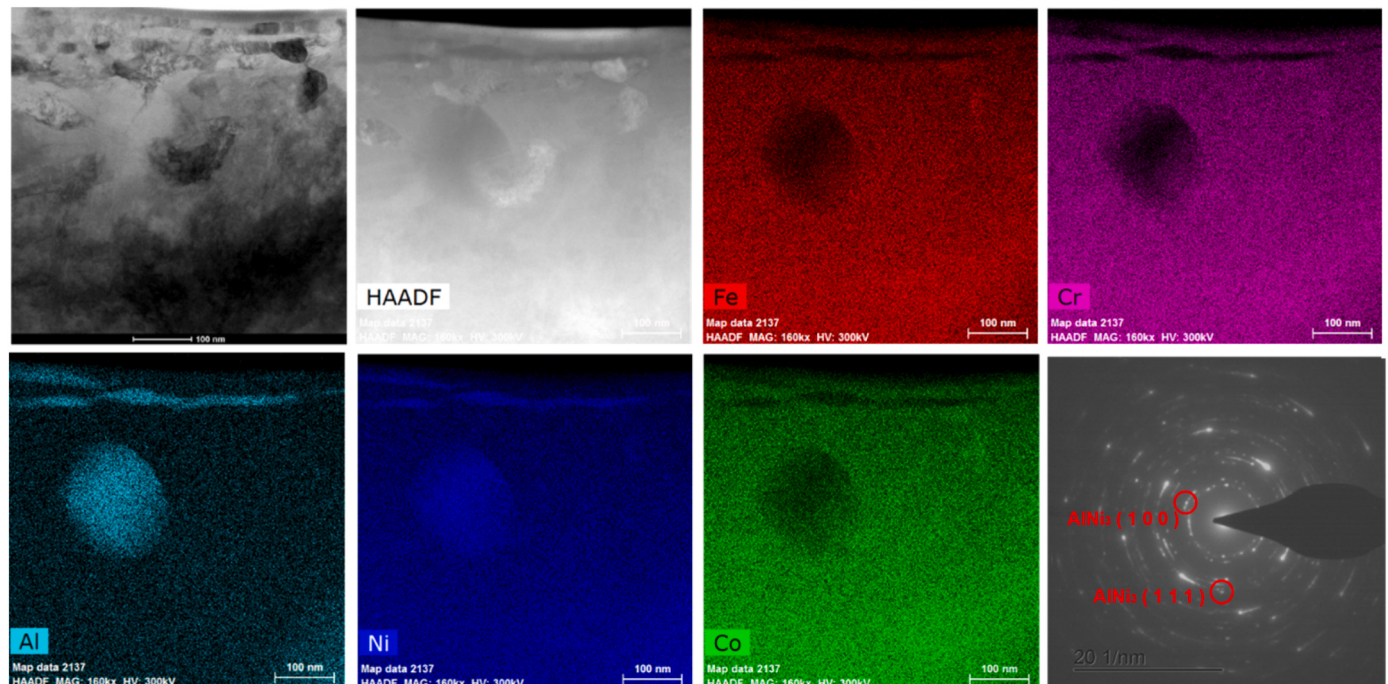


Fig. 5. Element mapping and diffraction pattern of CoCrFeNiAl0.3 after Fe + ion-irradiation at 300 °C to 1dpa.

These results suggest that Co and Ni would be distributed in the vicinity of vacancy-type defects or precipitates in non-irradiated CoCrFeNi-type HEAs. On the other hand, the lines of Al and Mn showed extremely lower intensity in the 5–20 momentum region, indicating that mono- or di-vacancies would be located with Al and Mn. Therefore, it is suggested that the vacancy migration barrier in CoCrFeNiMn and CoCrFeNiAl_{0.3} would be controlled by a strong interaction with Mn and Al, respectively. In addition, the interaction between Al and vacancies would be stronger than Mn according to the ratio curve in Fig. 3. These results would reasonably explain the change in the vacancy migration energy estimated by the in-situ electro-irradiation experiment in the chapter 3.1.

3.3. Irradiation-induced precipitates in HEAs

CoCrFeNiMn and CoCrFeNiAl_{0.3} were electron- and Fe⁺ ion-irradiated at 300–400 °C up to 1.5 dpa. Fig. 4 shows the elemental mapping around the precipitate in the electron irradiated CoCrFeNiMn. It clearly indicates that Co-, Ni-, and Fe-rich precipitate was observed in the irradiated CoCrFeNiMn. The diffraction spots and moiré fringe analysis also indicated the formation of the intermetallic compounds, such as FeCo and FeNi. On the other hand, Al- and Ni-rich precipitates were observed in the Fe⁺ ion-irradiated CoCrFeNiAl_{0.3} as shown in Fig. 5. The lattice spacing estimation and the EDS quantitative analysis revealed that the Al- and Ni-rich precipitate would be the intermetallic compound AlNi₃. In practice, a previous study indicated the formation of the ordered fcc L₁₂ intermetallic with a stoichiometry of AlNi₃ in CoCrFeNiAl_{0.3} after Kr + ion irradiated at 500 °C to 1.0 dpa [17]. B. Kombaiah et al. reported the formation of intermetallic compounds with complex structures in the phase diagram of various binary alloy systems formed from Co, Cr, Cu, Fe, and Ni [7]. This is a quaternary phase diagram of Co–Cr–Fe–Ni excluding Mn from CoCrFeNiMn estimated by first-principles calculation. On the other hand, a long-term annealing experiment of CoCrFeNiMn [18] revealed the precipitation of a BCC Cr-rich phase, a L₁₀ (Ni and Mn rich) phase, and a B2 (Fe and Co rich) phase were formed at 500 °C for 500 days. In the present study, the Fe³⁺ ion irradiation was performed at a lower temperature (300 °C) for a shorter time (1 h) compared with that in ref.17. Therefore, the precipitation of FeCo, FeNi, and Ni₃Al might be explained as a result of radiation-induced or radiation-assisted precipitation. While, from the result of positron annihilation measurement, there is a possibility of the Co- and Ni-rich phase formation prior to the irradiation experiments. Previously, L₁₂ nano-particles have been observed in as-cast Al_xCoCr-CuFeNi [19], as-cast [20] and 550 °C thermally-aged [21] Al_{0.3}CoCr-FeNi, suggesting that L₁₂ is stable phase at 550 °C, and likely also at 500 °C. In this study, however, none of precipitation was found in each HEA before the irradiation experiment. In order to better understand the precipitation behavior in HEAs under irradiation, well-designed analysis such as the long-term annealing under irradiation experiment could be needed.

4. Summary

In order to experimentally estimate the mobility of vacancy and interstitial in 316SS and CoCrFeNi-base high entropy alloys, the in-situ electron-irradiation experiment was performed. The vacancy migration energy in CoCrFeNiMn and CoCrFeNiAl_{0.3} was estimated to be lower and higher compared with that in 316SS, respectively. The higher vacancy migration energy in CoCrFeNiAl_{0.3} is probably due to a strong interaction between vacancy and Al. On the other hand, the loop

formation in HEAs was suppressed compared to that in 316SS. The positron annihilation analysis and the structure analysis indicated that the elements, such as Co, Ni, Mn, and Al atom, in HEAs could act an important role on the irradiation-induced microstructural evolution and the intermetallic compound precipitation. These results indicate that the excess vacancies produced during irradiation could be trapped by Co, Ni, and Al atoms in HEAs, leading to the delay of microstructural evolution and the enhancement of precipitation in HEAs.

Declaration of competing interest

The authors declare that they have no known competing financial interests or personal relationships that could have appeared to influence the work reported in this paper.

Acknowledgement

The authors appreciate the special support of Prof. Toyama at the Materials Research Institute at Oarai of Tohoku University for the positron annihilation measurement and the great helps of technical stuffs at HVEM and Nano-Micro Materials Analysis Laboratory of Hokkaido University. This work was supported by JSPS Grant-in-Aid for Scientific Research on Innovative Areas Grant Number JP19H05161.

References

- [1] J.-W. Yeh, S.-J. Lin, T.-S. Chin, J.-Y. Gan, S.-K. Chen, T.-T. Shun, C.-H. Tsau, S.-Y. Chou, Formation of simple crystal structures in Cu-Co-Ni-Cr-Al-Fe-Ti-V alloys with multiprincipal metallic elements, *Metall. Mater. Trans.* 35 (2004) 2533–2536.
- [2] Y.J. Zhou, Y. Zhang, Y.L. Wang, G.L. Chen, Solid solution alloys of AlCoCrFe-NiTi_x with excellent room-temperature mechanical properties, *Appl. Phys. Lett.* 90 (2007), 181904.
- [3] C.-Y. Hsu, J.-W. Yeh, S.-K. Chen, T.-T. Shun, Wear resistance and high temperature compression strength of Fcc CuCoNiCrAl0.5Fe alloy with boron addition, *Metall. Mater. Trans.* 35 (2004) 1465–1469.
- [4] C.-M. Lin, H.-L. Tsai, Equilibrium phase of high-entropy FeCoNiCrCu0.5 alloy at elevated temperature, *J. Alloys Compd.* 489 (2010) 30–35.
- [5] D.J.M. King, S.C. Middleburgh, A.G. McGregor, M.B. Cortie, *Acta Mater.* 104 (2016) 172–179.
- [6] B. Kombaiah, K. Jin, H. Bei, P.D. Edmondson, Y. Zhang, *Mater. Des.* 160 (2018) 1208–1216.
- [7] T. Nagase, Philip D. Rack, *joo hyon noh*, *Intermetallics* 59 (2015) 32–42.
- [8] S.J. Zinkle, G.S. Was, Materials challenges in nuclear energy, *Acta Mater.* 61 (2013) 735–758.
- [9] F.A. Garner, Radiation Damage in Austenitic Steels, in: R.J.M. Konings (Ed.), *Comprehensive Nuclear Materials*, Elsevier, Oxford, 2012, pp. 33–95.
- [10] S.Q. Xia, X. Yang, T.F. Yang, S. Liu, Y. Zhang, *JOM (J. Occup. Med.)* 67 (No. 10) (2015).
- [11] L.R. Owen, E.J. Pickering, H.Y. Playford, H.J. Stone, M.G. Tucker, N.G. Jones, *Acta Mater.* 122 (2017) 11–18.
- [12] M. Kiritani, *J. Nucl. Materials* 216 (1994) 220–264.
- [13] M. Kiritani, H. Takata, *J. Nucl. Materials* 69–70 (1978) 277–309.
- [14] S. Hayakawa, T. Okita, M. Itakura, T. Kawabata, K. Suzuki, *J. Mater Sci* 54 (2019) 11096–11110.
- [15] K. Toyota, Master thesis of Hokkaido university, 2020.
- [16] M. Elsayed, R. K-Rehberg, C. Eisenschmidt, B. Kieback, *Phys. Status Solidi A: Appl. Mater. Sci.* 215 (2018) 1800036.
- [17] Wei-Ying Chen, M.A. Kirk, N. Hashimoto, X. Jien-Wei Yeh, Liu Y. Chen, *J. Nucl. Mater.* 539 (2020) 152324.
- [18] F. Otto, A. Dlouhý, K.G. Pradeep, M. Kubanova, D. Raabe, G. Eggeler, E.P. George, *Acta Mater.* 112 (2016) 40–52.
- [19] C.-J. Tong, Y.-L. Chen, J.-W. Yeh, S.-J. Lin, S.-K. Chen, T.-T. Shun, C.-H. Tsau, S.-Y. Chang, Microstructure characterization of Al x CoCrCuFeNi high-entropy alloy system with multiprincipal elements, *Metall. Mater. Trans.* 36 (2005) 881–893.
- [20] T.-T. Shun, Y.-C. Du, Microstructure and tensile behaviors of FCC Al_{0.3}CoCr-FeNi high entropy alloy, *J. Alloys Compd.* 479 (2009) 157–160.
- [21] B. Gwalani, V. Soni, D. Choudhuri, M. Lee, J.Y. Hwang, S.J. Nam, H. Ryu, S. H. Hong, R. Banerjee, Stability of ordered L₁₂ and B2 precipitates in face centered cubic based high entropy alloys - Al_{0.3}CoFeCrNi and Al_{0.3}CuFeCrNi₂, *Scripta Mater.* 123 (2016) 130–134.